New constraints on mechanisms of remotely triggered seismicity at Long Valley Caldera

Emily E. Brodsky
Department of Earth and Space Sciences, University of California, Los Angeles, California, USA

Stephanie G. Prejean
Alaska Volcano Observatory, U.S. Geological Survey, Anchorage, Alaska, USA

Received 3 June 2004; revised 8 December 2004; accepted 6 January 2005; published 7 April 2005.

[1] Regional-scale triggering of local earthquakes in the crust by seismic waves from distant main shocks has now been robustly documented for over a decade. Some of the most thoroughly recorded examples of repeated triggering of a single site from multiple, large earthquakes are measured in geothermal fields of the western United States like Long Valley Caldera. As one of the few natural cases where the causality of an earthquake sequence is apparent, triggering provides fundamental constraints on the failure processes in earthquakes. We show here that the observed triggering by seismic waves is inconsistent with any mechanism that depends on cumulative shaking as measured by integrated energy density. We also present evidence for a frequency-dependent triggering threshold. On the basis of the seismic records of 12 regional and teleseismic events recorded at Long Valley Caldera, long-period waves (>30 s) are more effective at generating local seismicity than short-period waves of comparable amplitude. If the properties of the system are stationary over time, the failure threshold for long-period waves is ~0.05 cm/s vertical shaking. Assuming a phase velocity of 3.5 km/s and an elastic modulus of 3.5×10^{10}Pa, the threshold in terms of stress is 5 kPa. The frequency dependence is due in part to the attenuation of the surface waves with depth. Fluid flow through a porous medium can produce the rest of the observed frequency dependence of the threshold. If the threshold is not stationary with time, pore pressures that are >99.5% of lithostatic and vary over time by a factor of 4 could explain the observations with no frequency dependence of the triggering threshold.

Citation: Brodsky, E. E., and S. G. Prejean (2005), New constraints on mechanisms of remotely triggered seismicity at Long Valley Caldera, *J. Geophys. Res.*, *110*, B04302, doi:10.1029/2004JB003211.

1. Introduction and Overview

[2] Seismicity increased in Long Valley Caldera following the M_w = 7.9 2002 Denali Fault earthquake, M_w = 7.1 1999 Hector Mine earthquake and M_w = 7.3 1992 Landers earthquake. The three main shocks were 3460, 400, and 440 km from Long Valley, respectively [*Hill et al.*, 1993; *Gomberg et al.*, 2001; *Prejean et al.*, 2004].

[3] As pointed out by previous studies, in these long-range, rapid triggering cases, the seismic waves are the immediate cause of the earthquakes rather than the large-scale static stress change or viscoelastic stresses [e.g., *Hill et al.*, 1993; *Kilb et al.*, 2002]. This argument has been made for two reasons: (1) The seismic waves are the largest amplitude stresses resulting from the earthquakes at these distances. Static stresses at Long Valley for all of the earthquakes that triggered local seismicity are $\leq$100 Pa while the dynamic stresses are $>10^4$ Pa. (2) Triggered earthquakes begin with the arrival of the surface waves [e.g., *Prejean et al.*, 2004]. The key question that we address in this paper is what feature of the seismic waves determines if a given main shock triggers earthquakes at a given site.

[4] Since Long Valley has triggered repeatedly with intervals as short as 3 years, the system appears to recover to a state susceptible to triggering over a relatively short time. Further evidence for rapid recovery from triggering comes from a similar site, the Geysers geothermal field, which has had repeated triggering episodes as close as 2.5 months apart [*Stark and Davis*, 1996]. Long Valley Caldera is exceptionally well-instrumented with comparable on-scale broadband recordings for several large regional earthquakes that did and did not trigger local earthquakes. We use the Southern California Seismic Network (SCSN) station Mammoth Lakes (MLAC) for much of this study as it is the longest running broadband station in the caldera. The Northern California Seismic Network (NCSN) has a dense, short-period array in the area that allows us to definitively show an absence of increased number of local earthquakes above magnitude 1.2 following several moderate-sized regional earthquakes. We can examine

0148-0227/05/2004JB003211$09.00

Table 1. Earthquakes Studied[a]

Earthquake	M_w	Centroid Time, UT	Δ, km
Denali	7.9	3 Nov. 2002 2213:28	3457
Landers	7.3	28 June 1992 1157:34	438
Hector Mine	7.1	16 Oct. 1999 0946:59	397
Mendocino	7.0	1 Sept. 1994 1516:01	683
Northridge	6.7	17 Jan. 1994 1230:51	381
San Simeon	6.5	22 Dec. 2003 1916:06	302
Eureka Valley	6.1	17 May 1993 2320:54	102
Parkfield	6.0	28 Sept. 2004 1715:24.24	243
Double Springs Flat	5.9	12 Sept. 1994 1223:47	149
Northridge aftershock	5.8	17 Jan. 1994 2333:35	379
Ridgecrest	5.5	20 Sept. 1995 2327:42	355
Eureka aftershock	5.0	18 May 1993 2348:55	114

[a]Epicentral distance Δ is measured from earthquake epicenter to broadband station MLAC in Long Valley.

both catalogs and archived waveforms for any evidence of triggering. Therefore it is reasonable to look for a consistent threshold on the basis of some feature of the seismic waves for all of the earthquakes that have generated large shaking at Long Valley.

[5] We began this study by examining the triggering effects of all the earthquakes from June 1992 to October 2004 that produced $\geq$0.2 cm/s vertical shaking at the broadband station MLAC when the earthquake was at least 100 km away (Table 1). The value of the minimum shaking criteria was selected to ensure that a sampling of triggering and nontriggering earthquakes were in our data set. Although we have not checked every earthquake globally, we are aware of no evidence for any earthquake with weaker shaking than 0.2 cm/s triggering seismicity in Long Valley. We impose the minimum distance criterion in order to confine ourselves to situations where the stresses from the seismic waves, as opposed to the static stress field, is the most viable triggering stress. The results are not sensitive to the arbitrary 100 km cutoff as few earthquakes occur between 20 and 100 km from the seismic station. The Long Valley seismicity was investigated after each of 12 earthquakes that met the shaking and distance criteria. For every earthquake we used local catalogs, short-period waveforms and broadband waveforms to check for locally triggered events. Only the three earthquakes that previous studies had classified as triggering (Landers, Hector Mine and Denali) had any anomalous activity in the catalog or the waveform data. Every other earthquake had a normal number of cataloged events (<10 day) within 24 hours of the main shock and no more than one local earthquake during the passage of the seismic waves from the distant earthquake. More extensive characterization of the Landers, Hector Mine and Denali sequences can be found in previous work [*Hill et al.*, 1995; *Gomberg et al.*, 2001; *Prejean et al.*, 2004]. Using this information about which earthquakes triggered Long Valley as a starting point, this paper attempts to distinguish between the local ground shaking of the triggering and nontriggering earthquakes.

[6] Previous studies have suggested that large, distant earthquakes are more effective at triggering local seismicity than moderate regional ones [*Anderson et al.*, 1994]. This basic observation suggests that the duration or frequency content of the wave field may be important for determining the efficacy of triggering in addition to the amplitude of the waves. Here we use more recent data to more fully quantify this observation at Long Valley and then use those new observations to constrain the possible triggering mechanism.

[7] In this paper we evaluate three plausible thresholds for triggering at a site that is known to be sensitive to distant triggering: (1) the amplitude of the seismic waves, (2) the cumulative dynamic stress in the waves and (3) the amplitude in a certain frequency band. The absence or presence of each of these three types of thresholds is used to constrain the triggering mechanism at Long Valley Caldera. As will be shown below, we find that the first two possibilities do not explain the data at Long Valley Caldera, but the third does. The second half of the paper interprets these observations. We first evaluate the importance of the depth dependence of the wave field and show that a large portion of the frequency effect is due to attenuation of the surface waves with depth. After taking into account the depth effects, we are still able to extract some constraints on the mechanisms on long-range triggering. We then discuss how our observations contradict the predictions of some previously proposed triggering mechanisms and restrict the applicability of others. We proceed to show that adding the additional step of fluid flow in a porous medium matches the observations. If the fluid flow unclogs fractures and results in large pore pressure changes then frictional instabilities or subcritical crack growth could follow to produce earthquakes. We conclude by briefly discussing the general applicability of our findings to areas beyond Long Valley Caldera.

2. Possible Thresholds

2.1. Velocity Amplitude

[8] The dynamic stresses generated by a seismic wave are proportional to the particle velocity recorded by a seismometer [*Love*, 1927; *Jaeger and Cook*, 1979]. All proposed triggering mechanisms rely on some feature of the stress or strain fields of the seismic waves. Amplitudes ranging from 0.2 to 6 cm/s have been proposed as thresholds for distant triggering [*Brodsky et al.*, 2000; *Gomberg et al.*, 2001; *Prejean et al.*, 2004]. The key evidence against a simple amplitude threshold comes from the comparison of regional and more distant events in Long Valley Caldera. Figure 1 shows the peak amplitude shaking in Long Valley for the 12 events from 1992 to 2004 with comparable amplitude shaking ($\geq$0.2 cm/s). The magnitudes range from 5.0 to 7.9.

[9] Unfortunately, two of the documented triggering cases had problematic or missing records at the broadband

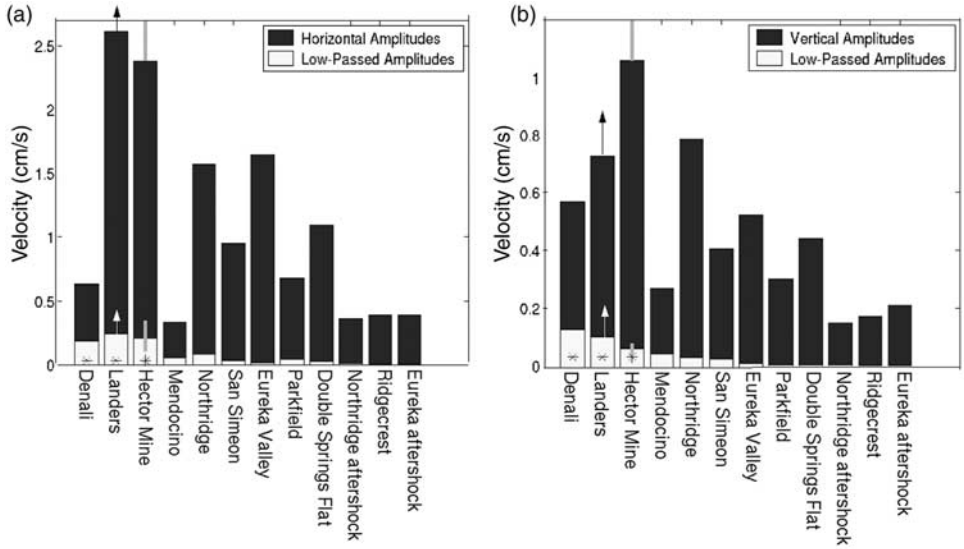

Figure 1. Peak amplitudes of (a) horizontal and (b) vertical seismograms recorded in Long Valley for triggering (starred) and nontriggering earthquakes. Earthquakes are listed in descending order of magnitude. Arrows indicate lower bounds for Landers as discussed in the text. Error bars for Hector Mine are based on the corrections for using a different seismometer site as discussed in Appendix A. The top error bar is so large that it is truncated in this figure so that the details of low-pass bars are not lost. The upper bound for the unfiltered Hector Mine shaking is 6.4 cm/s on the horizontal and 1.8 cm/s on the vertical.

station MLAC. For the Landers earthquake, the early prototype MLAC station failed 30 s after the arrival of the Love waves and before the peak of the Rayleigh wave motion. Therefore the recorded motion is a lower bound on the actual peak ground motion during the earthquake. During the Hector Mine earthquake, MLAC was nonoperational. For Hector Mine we substitute the record from the most comparable nearby station, Tinemaha (TIN), with appropriate corrections to account for attenuation, spreading, radiation pattern and site effects. Those corrections are detailed in Appendix A and the resulting error bars are included on Figure 1.

[10] Another potential instrumental problem is that the horizontal components of the seismometer may be responding nonlinearly to some of the largest ground motion. The new Guralp CMG-1T seismometer installed in December 2003 exceeds its linear range at a lower amplitude of shaking than the previously installed Streickeisen STS-2. The resulting horizontal amplitudes for the San Simeon and Parkfield earthquakes therefore are only an approximation of the actual ground motion for these two earthquakes. Fortunately, this problem does not affect our final conclusions as the subsequent analysis holds for the verticals as well as the horizontals.

[11] No clear threshold can be drawn separating either the peak horizontal or vertical amplitudes for the earthquakes that trigger local seismicity and those that do not (Figure 1). This conclusion holds even if the problematic Parkfield and San Simeon horizontal records are omitted. For the vertical amplitudes, the Northridge shaking exceeded Denali and Eureka Valley was comparable (<10% different). For the horizontals, Northridge, Eureka Valley and Double Springs Flat all exceed Denali, yet only Denali triggered.

[12] For instance, the M_w = 6.7 Northridge earthquake generated higher-amplitude shaking in Long Valley than the Denali earthquake (Figure 2), yet the Denali earthquake triggered seismicity and the Northridge earthquake did not. Following Northridge, there was no evidence of any local earthquakes in the waveforms and in the subsequent 24 hours there were only 10 cataloged events in Long Valley. (The probability of having 10 or more events on a given day in the caldera is 48%). In contrast, the Denali earthquake was followed by approximately 60 Long Valley earthquakes within 15 min of the arrival of the surface waves. The data for this specific case combined with the more general results of Figure 1 implies that amplitude of particle velocity is not a good discriminant for triggering.

2.2. Duration and Energy

[13] Physical arguments suggest that either the duration of shaking or the cumulative stress in the wave field, i.e., energy density, could potentially be a useful threshold [*Hill et al.*, 1993; *Sturtevant et al.*, 1996; *Brodsky et al.*, 2000]. We first examine duration as a threshold by observing the timing of local earthquakes relative to the wave train of the distant, triggering main shock. After Landers, the first local earthquake at Long Valley appears $\sim$15 s after the beginning of the surface waves. If duration is the key criterion, strong shaking that lasts at least 15 s ought to be sufficient to trigger events from other main shocks. The strong surface wave shaking for Northridge lasted 25 s, yet no triggering occurred. Therefore it appears as if duration might not be a relevant threshold.

[14] A more robust test of the cumulative effect of the seismic waves is to calculate the energy density in the

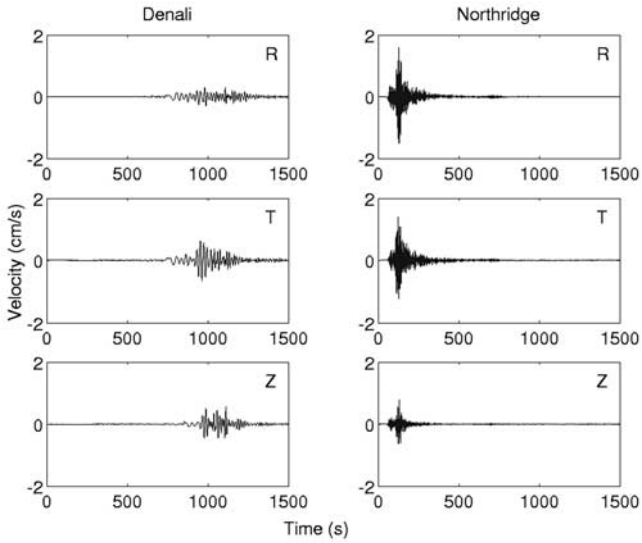

Figure 2. Seismograms for the Denali and Northridge earthquakes at Long Valley. The radial (R), transverse (T), and vertical (Z) components are as labeled. The Denali earthquake triggered local seismicity and Northridge did not.

wave field of large distant earthquakes. Integrated energy density E measures the cumulative stressing and is defined as

$$E = \rho c \int \dot{u}^2 dt, \tag{1}$$

where ρ is the local rock density, c is the phase velocity, and $\dot{u}$ is the particle velocity. Although energy density as specifically defined by equation (1) is not necessarily the predicted threshold for many mechanisms, it provides a general and physically based measure of duration and cumulative shaking. Figure 3 shows that the local triggering during Denali occurred at the beginning of the surface wave train when the cumulative energy density that had passed through Long Valley was still <200 J s/m^2 where c is approximated by a constant value of 3.3 km/s. If energy density were an appropriate measure of the threshold, then the four regional events shown should have also triggered local seismicity (Figure 3). They did not. Seismicity also began early in the wave trains for other sites triggered by Denali. The triggered swarms at both the Geysers and Coso geothermal field began with $E < 40$ J s/m^2.

2.3. Frequency

[15] Although the observed total amplitude of strain does not seem to be the correct threshold for triggering, it is

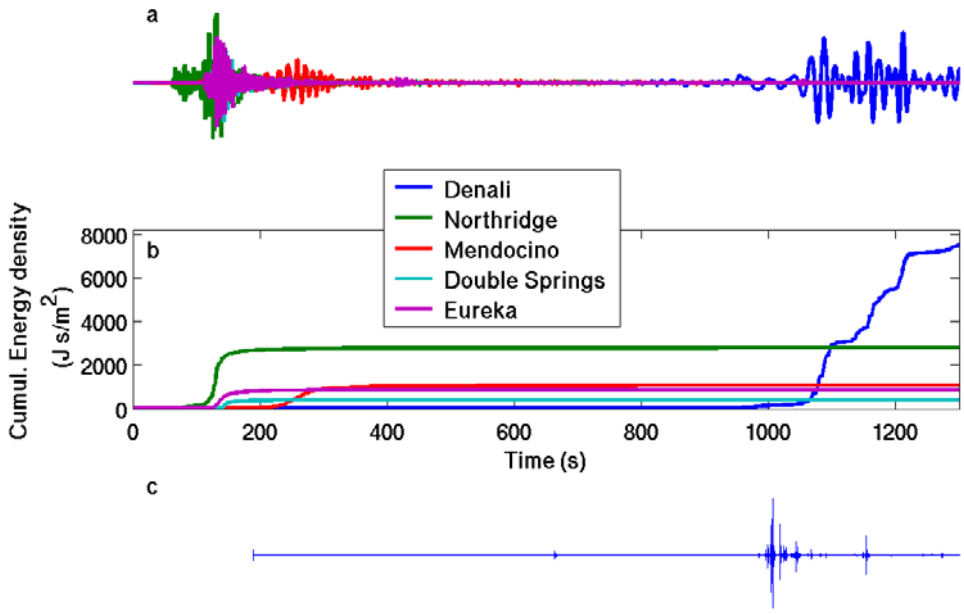

Figure 3. Comparison of cumulative energy and timing of triggered events. (a) Vertical MLAC seismograms from Long Valley for five earthquakes. (b) Cumulative energy density E (equation (1)). (c) High-frequency (>7 Hz) filter of nearby (<15 km away) OMM vertical seismograms showing locally triggered events for Denali earthquake. Triggering begins for Denali at the dotted line when the energy is less than 200 J s/m^2, which is a value less than the energy in the waveforms of the three regional events shown. The other three traces are for regional events that did not trigger any earthquakes in Long Valley. The small magenta signals in the middle of the records in Figure 3a are aftershocks of Eureka originating in the source region; that is, they are not locally triggered events. Magnitudes and distances for all earthquakes are given in Table 1.

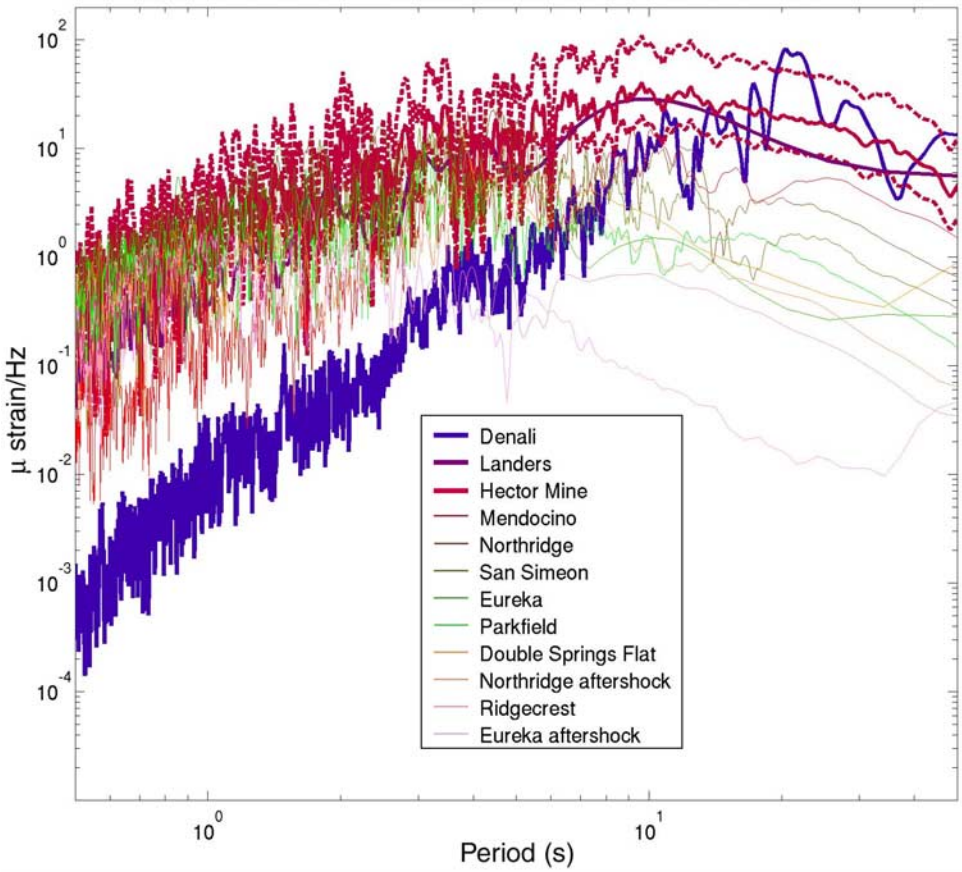

Figure 4. Spectra of the transverse components at Long Valley for the 12 earthquakes considered in this study. The thick lines indicate earthquakes that triggered local seismicity. A similar figure cannot be made for radial or vertical components because the Landers record is truncated before the Rayleigh waves. The spectrum from Hector Mine is bounded by the dashed lines to account for the extrapolation from TIN to MLAC. The dashed lines are the lowest and greatest correction factors for any frequency considered; that is, they bound the range of 0.5–2.7 times the observed record at TIN.

possible that the amplitude of the waves in a particular frequency band is the correct parameter. The earthquakes that triggered had the highest long-period (>30 s) amplitudes (Figure 4), in part because they were large magnitude events.

[16] We isolate the long-period component of the shaking by filtering the observed seismic records with a low-pass filter with a corner frequency at 0.033 Hz (30 s). The peak amplitudes of the seismic records after they have been low-pass filtered are shown in Figure 1. After this filtering, we are able to define a threshold on the verticals bounded by Hector Mine and Mendocino between 0.04 and 0.08 cm/s with the range largely determined by the error bar on the Hector Mine shaking. Therefore we conclude that the appropriate threshold for triggering at Long Valley is the amplitude of the long-period waves (>30 s). If the data are filtered using a longer-period corner, then the distinction between the triggering and nontriggering earthquakes becomes even clearer.

[17] Since the triggering by Denali begins early in the wave train as shown by Figure 3, the comparison of the peak, unfiltered amplitudes of Northridge and Denali in Figure 1 is overly conservative. The amplitude of the vertical shaking at the beginning of the Denali triggering is ~0.15 cm/s which is 20% the peak amplitude of the Northridge vertical component. This observation reinforces the conclusion that if amplitude were the physically relevant threshold, then Northridge should have triggered local earthquakes in Long Valley. When the frequency content is limited to wavelengths with periods longer than 30 s, the Northridge vertical component amplitude is less than the amplitude of the Denali waves at the time of triggering.

[18] The early triggering can also be taken as further evidence for frequency dependence in a different way. The dispersed Rayleigh wave train has the longest-period waves arriving at the station first. Therefore, if the longest-period waves are most effective at triggering, we would expect the triggering to occur at the beginning of the Rayleigh wave packet. It does.

[19] The low-pass filter in velocity can alternatively be interpreted as a displacement threshold of 1.1–1.6 cm vertical displacement. However, no currently developed or quantified model suggests a displacement threshold rather

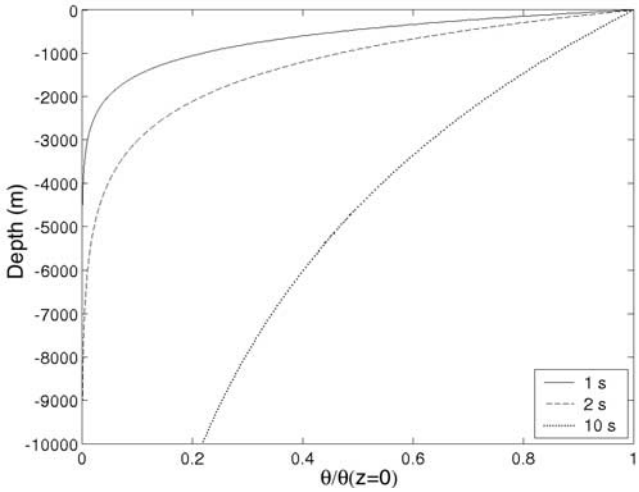

Figure 5. Standard Rayleigh wave decay with depth curves for dilatational strain, θ, normalized by the value at the surface, $\theta(z = 0)$ [*Ben-Menahem and Singh*, 1981]. Phase velocity is 3.5 km/s. The curves represent the strain as a function of depth for different surface wave periods (as labeled).

than a strain or stress one. Perhaps the results of this study may motivate the investigation and discovery of displacement-dependent triggering mechanisms.

3. Interpretations

3.1. Depth

[20] One factor that may contribute to the relative effectiveness of the long-period waves in triggering earthquakes is the depth of the triggered earthquakes. The largest amplitude shaking is from the surface waves and the amplitudes of surface waves are less at depth than at the surface. The highest-frequency surface wave amplitudes decrease most rapidly as a function of depth (Figure 5). Since the triggered earthquakes occur below the surface, we expect the amplitude of the surface waves at the triggered hypocenters relative to the surface measurements to depend on the frequency. Here we evaluate the possibility that low-frequency waves trigger earthquakes more easily simply because the earthquakes are triggered at depths deeper than the high-frequency surface waves can penetrate.

[21] Twenty percent of the located triggered earthquakes at Long Valley occur at very shallow depths ($\leq$3 km). At these depths for most surface wave frequencies, the loss of energy relative to the observed surface waves is fairly modest. The frequency dependence for deeper triggered events (>8 km) may be due entirely to the decay of the surface waves. However, we must explain both the deep and shallow triggered seismicity. Since the frequency dependence of the deep events is relatively easy to explain and has no resolving power on mechanism, we focus on the shallow triggered events as the ones that can resolve a frequency dependence in the triggering mechanism.

[22] Figure 6 shows the amplitudes corrected with standard frequency-dependent surface wave corrections to 3 km depth. For the Love waves, we solve for the frequency-dependent phase velocities and amplitude corrections by using a simplified version of the standard USGS Long Valley velocity with a 50% increase in the S wave velocity at 3 km [*Ben-Menahem and Singh*, 1981]. For the Rayleigh waves, we use a constant phase velocity c = 3.5 km/s and the standard depth dependence in Figure 5.

[23] After correcting for depth, we still require further low-pass filtering to separate the amplitudes of the triggering from the nontriggering earthquakes. This result holds for both the verticals and horizontals. For instance, on the verticals the Northridge earthquake had larger amplitude shaking at 3 km depth than Denali. Since the Northridge amplitude is only 20% higher than the Denali one and no other nontriggering earthquake produced comparable vertical shaking at depth, the requirement for low-pass filtering in Figure 6b is less robust than the requirement in Figure 1b. However, as discussed before, there is another piece of evidence for the importance of the low-frequency waves. Local earthquakes are triggered by the long-period, low-amplitude waves arriving early in the surface wave train. The early wave train triggering cannot be explained by simple depth dependence. For this reason, we pursue the possibility that the mechanism that generates the shallow triggered seismicity appears to have a frequency dependence in addition to the seismological filtering of the waves with depth.

3.2. Triggering Mechanism

[24] Several mechanisms for dynamic triggering of earthquakes have previously been proposed. The most quantitatively developed classes of mechanisms are bubble pressurization, rate and state friction, subcritical crack growth, and fracture unclogging. Here we briefly review the physics of each mechanism, discuss potential problems and highlight whether or not we expect strong amplitude, duration or frequency dependence in each case. Our discussion of rate and state friction is the most detailed because of the model's widespread use in the literature.

3.2.1. Bubble Pressurization

[25] Since triggering is commonly observed in geothermal areas, some researchers have suggested that the seismic waves pressurize the multiphase geothermal fluids and the pressurization results in earthquakes. Two types of bubble pressurization mechanisms have been proposed. Rectified diffusion pumps volatiles into bubbles over successive strain cycles [*Sturtevant et al.*, 1996; *Brodsky et al.*, 1998]. Advective overpressure occurs when bubbles are shaken loose inside a magma chamber and proceed to rise [*Linde et al.*, 1994]. In the latter mechanism, the rising bubbles cause the pressure of the magma body at the level of the bubbles to equilibrate with the pressures formerly found at the depth of the bubbles' origin, therefore the total pressure of the chamber increases if the bubbles have traversed a significant vertical distance. Both mechanisms suffer from the same theoretical problem, i.e., as the bubbles pressurize the surrounding fluid, they resorb and therefore cease to increase the pressure. The limiting pressure will be very low except in exceptional circumstances such as an oversaturated magma chamber that is constantly degassing at a rate exactly balanced by the new gas exsolved by crystallization [*Brodsky*, 2001; *Ichihara et al.*, 2003]. Nevertheless, it could be argued that these special circumstances exist in

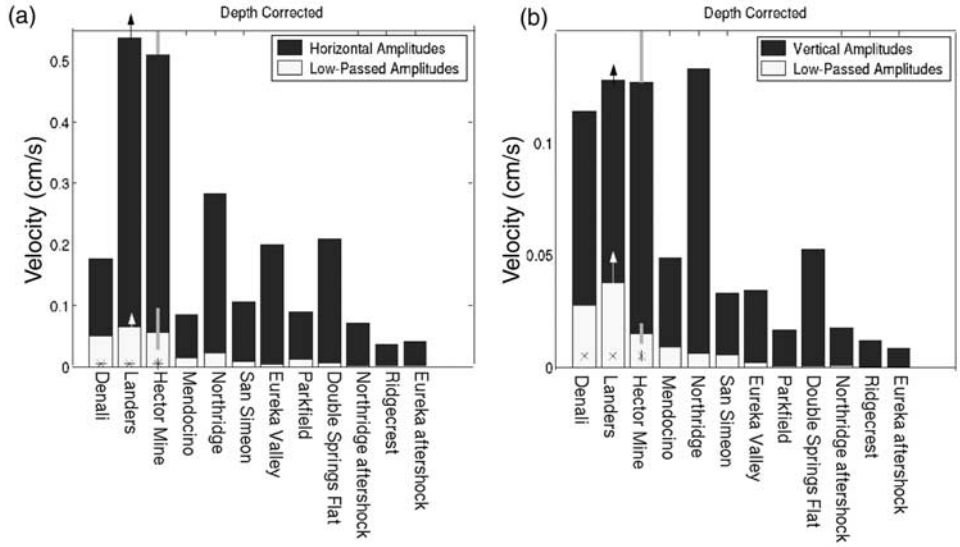

Figure 6. Peak amplitudes (a) horizontal and (b) vertical of seismograms corrected to 3 km depth in Long Valley for triggering (starred) and nontriggering earthquakes. Arrows are lower bounds as discussed in text, and error bars are calculated the same as in 1. The upper bound of the unfiltered horizontal Hector Mine error bar is 0.22 cm/s.

a complex and constantly evolving magma chamber [*Brodsky et al.*, 1998].

[26] Direct observational evidence for or against these mechanism is a more robust way to confirm or refute the possibilities. The rectified diffusion model predicts that the pressurization depends on the square of the seismic wave amplitude. Rectified diffusion should also depend linearly on the duration of shaking and therefore directly on the energy as defined in equation (1). No other frequency dependence is expected. The rectified diffusion model contradicts the observations in all three dependencies: amplitude, energy and frequency. For advective overpressure, the amplitude dependence is not specified, but it is expected to be strongly nonlinear as the process involves shaking loose marginally stable bubbles. Advective overpressure as currently formulated has no explicit period or duration dependence [*Linde et al.*, 1994]. The advective overpressure mechanism contradicts our observations in requiring a risetime for the bubbles and therefore delay of seismicity. In contrast, triggered seismicity is observed early in the wave train.

3.2.2. Rate and State Friction

[27] Rate and state friction provides the most thoroughly explored quantitative model for failure during the passage of the seismic waves [*Dieterich*, 1994; *Gomberg*, 2001; *Perfettini et al.*, 2003]. In the model, the seismic waves promote instabilities by temporarily stressing appropriately oriented faults and prompting a run away reduction of the velocity- and history-dependent frictional stress. Rate and state models must invoke some ancillary process like a local creep event to explain sustained triggering [*Gomberg*, 2001]. *Perfettini et al.* [2003] showed that there are some parameter regimes in which dynamic triggering of rate-state instabilities produces immediate earthquakes in the wave train. The amplitude, duration and frequency dependencies studied here provide constraints on whether or not those regimes are applicable to the natural system. Below we show that the rate and state model can only explain the increase in seismicity from the observed stressing if the pore pressures are very high and variable with time.

[28] In the rate and state model, the increase in the number of local earthquakes is strongly dependent on the amplitude of the applied stress. For a fault approaching failure, an exponential dependence arises because the change in slip velocity due to a shear stress step of $\Delta\tau$ on a fault is

$$\dot{\delta}_+ = \dot{\delta}_- \exp(\Delta\tau/A\sigma), \tag{2}$$

where $\dot{\delta}_+$ is the slip velocity after the stress is imposed, $\dot{\delta}_-$ is the slip velocity before, A is the rate-state parameter that governs velocity strengthening and σ is the background normal stress [e.g., *Dieterich*, 1994, equation (A17)].

[29] We approximate the background normal stress as the effective stress given by

$$\sigma = \sigma_0 - p_p, \tag{3}$$

where σ_0 is the lithostatic pressure and p_p is the pore pressure [*Hubbert and Rubey*, 1959]. In this simplification, the variations of σ at a given depth are due to variations in p_p. Long-range triggering is more commonly observed in geothermal areas than tectonic settings even when there are comparable stresses and very dense monitoring instrumentation available in both areas [*Spudich et al.*, 1995]. The rate and state models explain the prevalence of geothermal triggering by proposing that geothermal areas have unusually low normal stresses due to near-lithostatic hydrothermal fluids [*Perfettini et al.*, 2003]. We will use the observed seismograms to calculate how high the fluid pressure in Long Valley must be to explain the observed seismicity increase.

[30] The applied stress $\Delta\tau(t)$ is proportional to the particle velocity $\dot{u}(t)$ in the depth-corrected seismograms. We used the conversion $\Delta\tau = \mu\dot{u}/c$, where μ is the shear

modulus and c is the phase velocity. For simplicity, we assume that c is constant and use the vertical component for $\dot{u}$. For typical values of μ and c, the stresses from the depth-corrected Denali seismic waves are on the order of 0.01 MPa.

[31] If rate and state friction is the dominant mechanism promoting triggering and the background stress does not change with time, on the basis of the nonlinear equation (2) we expect a large increase in the number of events triggered over a small range of triggering stresses, i.e., a threshold-like behavior. Such a threshold is not observed for Long Valley even in the depth-corrected data. In Figure 6, Northridge has a ~20% higher peak stress than Denali unless an additional low-pass filter is applied. As will be discussed below, the rate and state model by itself does not include any such filter. Therefore the rate and state model with a constant effective stress cannot explain the data; however, a variable effective stress can. Variations of only 20% in σ can account for the 20% difference in apparent triggering thresholds between Northridge and Denali. From equation (3), the change in effective stress $\Delta\sigma$ due to a change in pore pressure Δp_p is

$$\frac{\Delta\sigma}{\sigma} = \frac{\dfrac{-\Delta p_p}{p_p^0}}{\dfrac{\sigma_0}{p_p^0} - 1}, \tag{4}$$

where p_p^0 is the initial pore pressure. Equation (4) shows that if the initial pore pressure p_p^0 is close to the lithostatic stress σ_0, then large changes in effective stress result from modest changes in pore pressure. On the other hand, if $\sigma \gg p_p^0$, very large changes in pore pressure are necessary to change the effective stress. We must now proceed to constrain the pore pressure in order to evaluate whether the effective stress can change enough to explain the data.

[32] We calculate the integrated effect of shaking on the rate and state model as a way to constrain the pore pressure. Rate and state models predict that the longer the shaking continues, the greater the triggering potential [*Perfettini et al.*, 2003]. We show in Figure 3 that no dependence on cumulative energy is observed for Long Valley. Earthquakes are triggered early in the wave train, even though the total energy that has passed is low relative to the nontriggering earthquakes. Now we construct a figure similar to Figure 3 for the rate-state predicted integrated seismicity rate change. The excess number of events E_{RS} at time t relative to the expected number of events is

$$E_{RS} = \int_0^t R(\hat{t})d\hat{t} - r_0 t = r_0 \int_0^t \frac{\gamma_0}{\gamma(\hat{t})}d\hat{t} - r_0 t, \tag{5}$$

where R is the instantaneous seismicity rate, r_0 is the background seismicity rate, γ is the rate evolution parameter of *Dieterich* [1994] and γ_0 is the value of γ at time 0. *Dieterich* [1994] derives that γ evolves under an arbitrary shear stress function as

$$d\gamma = \frac{1}{A\sigma}(dt - \gamma d\tau). \tag{6}$$

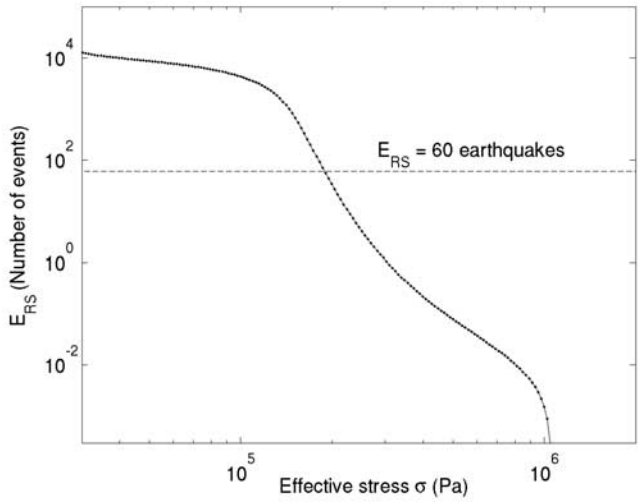

Figure 7. Number of excess events predicted by the rate and state model for the Denali earthquakes as a function of assumed effective stress σ. Parameters are $A = 0.005$, $r_0 = 9$ earthquakes per day, $c = 3.5$ km/s and $\mu = 3.5 \times 10^{10}$ Pa. Dashed line shows the minimum number of earthquakes observed during the Denali wave train.

If the stressing term is much more important than time-dependent term on the right-hand side of equation (6), then E_{RS} reduces to an integration of equation (2):

$$E_{RS} \approx r_0\left(\int_0^t \exp(\tau(\hat{t})/A\sigma)d\hat{t} - 1\right). \tag{7}$$

[33] Figure 7 shows E_{RS} calculated from the full equations (2)–(6) as a function of σ. For r_0 we use the median seismicity rate at Long Valley which is 9 earthquakes/day (10^{-4} earthquakes/sec). The rate-state parameter A is typically ~0.005 although some studies suggest higher values of A for hydrothermal conditions [*Roy and Marone*, 1996; *Blanpied et al.*, 1995]. We pick the lower value of A in order to find the maximum value of σ given a constraint on the combination of parameters $A\sigma$.

[34] There were at least 60 earthquakes observed at Long Valley during the Denali wave train. Using Figure 7, the observed number of earthquakes requires σ to be no more than 0.19 MPa. From equation (3), this value of σ requires that the pore pressure is more than 99% of lithostatic at 3 km. The pore pressure result is robust to reasonable variations in the parameters A and r_0 because Figure 7 shows that the number of expected events falls precipitously for any effective stress much greater than $\Delta\tau/A$. In order to have any significant number of rate-state triggered events, p_p must be large enough that $A\sigma$ is close to the imposed stress from the seismic waves.

[35] We now use the full equation (5) to constrain the variations in effective stress necessary to have sufficiently variable thresholds at the times of different earthquakes for the rate and state model to match the data. Figure 8 shows that the cumulative shaking even from the depth-corrected seismograms is predicted to have produced more of an effect (higher E_{RS}) from Northridge, Mendocino, Double Springs and Eureka than the cumulative shaking at the

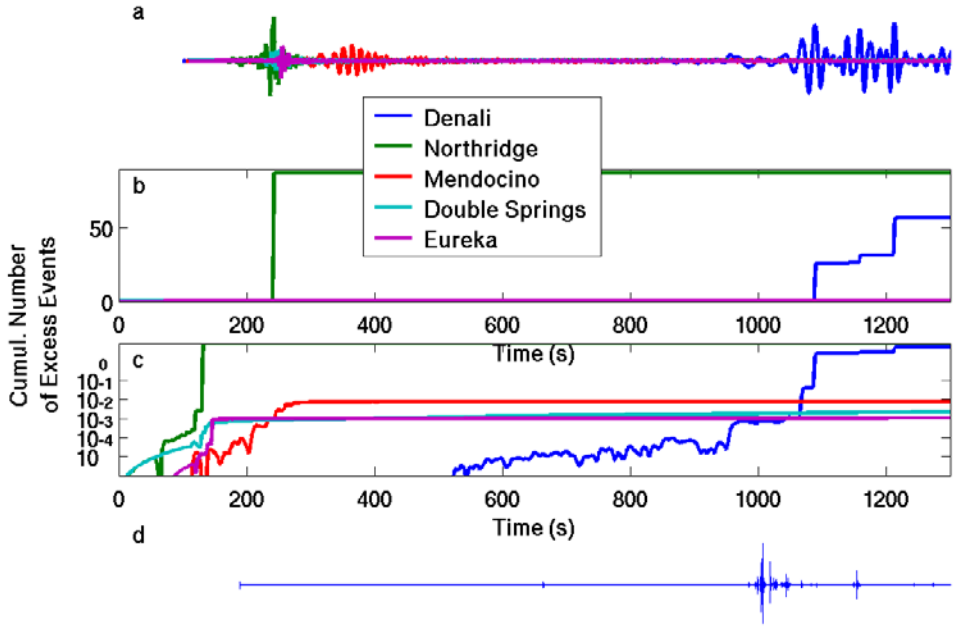

Figure 8. Cumulative number of excess earthquakes predicted by the rate and state model in equations (5)–(6). (a) Vertical MLAC seismograms corrected to 3 km, (b) E_{RS} from equation (5) and the depth-corrected seismograms in Figure 8a, (c) same curves as in Figure 8b plotted with a logarithmic y scale to show differences at small values, and (d) high-frequency (>7 Hz) filter of nearby (<15 km away) OMM vertical seismograms showing locally triggered events for Denali earthquake. Parameters are $A = 0.005$, $\sigma = 0.19$ MPa, $r_0 = 9$ earthquakes per day. γ_0 is arbitrary and does not affect the value of E_{RS}.

time of the initiation of triggering from Denali (Figure 8c). In order for E_{RS} to be less at the time of the Denali triggering than the value of E_{RS} at the times of non-triggering, the effective normal stress at time of the Denali earthquakes would have to be a factor of 3 less than that during Mendocino and a factor of 4 less than during Northridge. Referring back to equation (4), the entire range of effective stresses requires less than 1% change in pore pressure if the initial pore pressure is within 99.5% lithostatic. These changes in effective stress could also be accommodated by changes in the tectonic driving stress.

[36] An alternative to having a temporally variable amplitude threshold is to have a low-pass filter that takes effect before rate and state failure begins. The calculation in Figure 8 accounts for any filtering effect inherent in the rate-state model by performing the full calculation of equations (5)–(6). Since E_{RS} is lower for Denali than Northridge for reasonable parameters, there is insufficient filtering in the rate-state model to explain the observed triggering with a constant effective stress. This result is consistent with previous work on the frequency dependence of the rate and state model [*Perfettini et al.*, 2003].

[37] To summarize, rate-state is consistent with our observations if there is a time-varying frequency-independent amplitude threshold due to small (<1%) changes in pore pressure, provided that the original pore pressure is within 99.5% of lithostatic in at least some areas of the caldera.

3.2.3. Subcritical Crack Growth

[38] Subcritical crack growth is the slow propagation of incipient fractures that are too small to propagate unstably with seismic velocities. One of the primary mechanisms for subcritical crack growth is stress corrosion, which is the weakening of the crack tip by reactions between the silicate rocks and water [*Atkinson*, 1984]. Geothermal areas are particularly subject to subcritical crack growth because of the abundance of corrosive fluids. Like rate and state friction, subcritical crack growth should also have a strong amplitude dependence. The analogous equation to equation (2) is

$$V_+ = V_-(1 + d\tau/\sigma)^p, \tag{8}$$

where V_- and V_+ are the crack propagation velocities before and after the imposed stress, respectively, and p is an empirical growth exponent that is measured by laboratory experiments to be at least 10 and is more commonly measured to be 20–40 for rocks [*Atkinson*, 1984; *Kanamori and Brodsky*, 2004]. In the limit of small oscillatory stresses compared to the background stress ($d\tau \ll \sigma$), a Taylor expansion, integration and some rearrangement of equation (8) yields

$$V \approx V_0 \exp(p\Delta\tau/\sigma), \tag{9}$$

where V_0 is the crack velocity with no stress and $\Delta\tau$ is the total change in stress. Equation (9) is identical to equation (2) to within a constant. An alternative derivation is to assume p is large and impose no restrictions of $\Delta\tau$. This alternative strategy is pursued in Appendix B to show that the full governing equations are mathematically identical for both the rate-state and stress corrosion systems.

With identical governing equations, the rest of the model predictions follow, i.e., subcritical crack growth can also explain the triggering given sufficiently high pore pressure if the effective stress changes with time. The stress corrosion parameter $1/p$ is analogous to the rate-state variable A. Since $1/p$ is typically an order of magnitude higher than the usual values for A, the required background effective stress to get significant triggering by stress corrosion is an order of magnitude lower than for rate and state. The required pore pressures are therefore correspondingly higher and differ from lithostatic by less than 0.1%. Again, these pore pressures are extreme, but theoretically possible. There is no inherent low-pass filter effect in the stress corrosion mechanism.

3.2.4. Unclogging Fractures

[39] Unclogging fractures is a possible additional stage in the triggering process. The seismic waves may drive a flow that flushes temporary blockages from fractures and faults therefore redistributing pore pressure [*Brodsky et al.*, 2003]. In this scenario, the seismogenic zone is envisioned as a hydrological system where constant precipitation and material transport can temporarily block fractures and cause isolated pockets of heterogeneous pore pressure before the waves clear the barriers and allow the pore pressure to reequilibrate rapidly. Under the unclogging scenario, the triggering process has three distinct stages: (1) driving the flow through the porous medium (2) removing the blockage and (3) reducing the effective stress on a section of a fault sufficiently to start an earthquake. Stages 2–3 may introduce strong dependence on the amplitude of the seismic waves and may involve some of the processes discussed above, however, the amplitude dependence takes effect only once the signal has passed through stage 1. If the flow through the porous medium introduces a low-pass filtering, then the triggering threshold is only sensitive to the long-period amplitudes and energies. Below we discuss in detail how flow through a porous medium generates this type of filter. We do not present here a complete model for how that flow ultimately generates earthquakes. A more thorough discussion of how flow removes blockages is given by *Brodsky et al.* [2003]. Once the blockage is removed and large pore pressure changes have been rapidly achieved, earthquakes can begin by frictional instabilities or subcritical fracture growth. The magnitude of the pore pressure held by the blockages is unconstrained by the current data and therefore that aspect of the model is untestable at this time.

3.2.5. Fluid Flow as a Low-Pass Filter

[40] The dilatational seismic strain θ induces different hydraulic heads in faults and the surrounding rock due to differences in poroelastic compressibilities (specific storage). The resulting gradient in head results in flow through the porous medium. We calculate the full flow resulting from the seismic waves for the case of an infinite planar fault embedded in a homogeneous, isotropic aquifer in Appendix C. The solution for the amplitude of the hydraulic head oscillation in the fault in terms of the imposed dilatational strain in the seismic wave is

$$\left|\frac{H_*}{\theta_\infty}\right| = \frac{1}{S_s^f}\frac{\frac{\sqrt{i\omega\kappa_r}}{b} + i\omega}{\frac{\sqrt{i\omega\kappa_r}}{b}\frac{S_s^r}{S_s^f} + i\omega}, \tag{10}$$

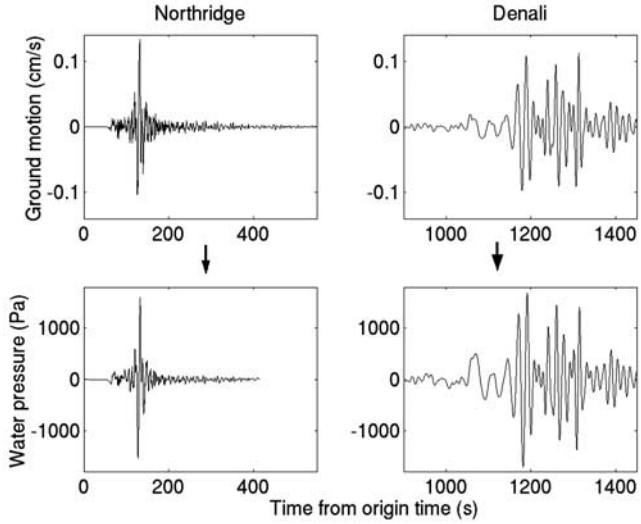

Figure 9. Vertical component of ground motion corrected to 3 km depth and computed water pressure records. Arrows connect the seismogram (input) to the synthetic water pressure record (output). The synthetics are computed by convolving the depth-corrected seismograms with the frequency response in equation (10) and the following parameters: specific storages $S_s^r = 10^{-8}\ \mathrm{m}^{-1}$, $S_s^f = 10^{-4}\ \mathrm{m}^{-1}$, fault half aperture $b = 1$ cm; and rock hydraulic diffusivity $\kappa_r = 10\ \mathrm{m}^2/\mathrm{s}$.

where H^* is the amplitude of the head oscillation in the fault, θ_∞ is the amplitude of the seismic strain oscillation, b is the fault damage zone half thickness, ω is the angular frequency of the seismic waves, κ_r is the hydraulic diffusivity of the wall rock and S_s^r and S_s^f are the specific storages of the wall rock and fault zones, respectively.

[41] Whenever the storage in the fault is large compared to the intact rock ($S_s^f b \gg S_s^r\sqrt{\kappa_r/\omega}$) and the diffusive boundary layer in the wall rock is much larger than the fault thickness ($\sqrt{\frac{\kappa_r}{\omega}} \gg b$), equation (10) simplifies and the amplification is a low-pass filter with $H_*/\theta_\infty \sim \sqrt{\frac{1}{\omega}} \sim \sqrt{T}$ where T is the period of the waves.

[42] The solutions shown in Figure 9 for the realistic parameters in the caption illustrate how the longer-period seismogram of Denali generates a 10% higher-amplitude pressure oscillation than Northridge. This is the requisite physical effect. The higher pore pressures during Denali will promote more flushing of fractures and greater subsequent pore pressure rearrangement than during Northridge. The ensuing nonlinear processes are not fully modelled here. The main result of this work is that there exists a physical variable (pore pressure) that can be higher for Denali than Northridge and therefore movement of pore fluid through the porous medium is a viable intermediary step to introduce frequency dependence.

[43] A failing of this model is that although the early long-period wave train is more prominent in the pressure trace than the seismogram, it still not higher than the peak Northridge pressure. The pore pressure model explains more of the data than any other model, but even this model does not explain everything. We emphasize here that the

pore pressure model captures the qualitative behavior of the observations, i.e., the low-pass filter.

[44] Although the above calculation is done for a restrictive geometry and specific set of parameters, the low-pass filter effect is a more general feature of flow through porous media into compressible faults. Aqueous fluid is abundant in the geothermal system. Evidence for highly compressible, partially saturated fractures at depth comes from attenuation studies using the Long Valley deep borehole. Borehole televiewer and temperature logs indicate that fluid filled fracture zones of $\leq$12 m width exist to depths of at least 2 km in Long Valley. The ratio of P wave Q to S wave Q suggests that compression-induced pore fluid flow is a significant source of attenuation at these depths as theoretically suggested by *Winkler and Nur* [1982].

[45] The general scaling between pressure oscillation amplitude ΔP and period of the wave T can be derived from the combination of three relationships:

$$\Delta P \propto \Delta V \sim uT, \tag{11}$$

$$u \propto \nabla h \sim \left(h_r - h_f\right)/L, \tag{12}$$

$$L \propto \sqrt{\kappa_r T}. \tag{13}$$

Equation (11) states that the pressure amplitude is proportional to the volume of water ΔV that is squeezed in and out of the fault during a period which in turn is proportional to the fluid velocity u multiplied by the period T. Equation (12) is Darcy's law where h is the hydraulic head, h_f and h_r are the heads in the fault and wall rock, respectively. The difference in head between the fault and the rock is supported over a length scale L, which is a diffusive boundary layer width (equation (13)). Combining equations (11)–(13),

$$\Delta P \propto T^{1/2}. \tag{14}$$

Even though equation (14) is a linearization that neglects interrelationships between equations (11)–(12), it is useful to provide a simple physical justification for the low-pass filtering of the flow that occurs over a wide range of parameters and geometries. Note that the frequency filter is a relatively weak function of T, therefore we do not expect a strong cutoff frequency for triggering. The low-pass filters used here provide amplitude thresholds for particular frequency bands. They are not meant to be interpreted as thresholds in frequency.

4. Generalization Beyond Long Valley

[46] Since the observations presented here are at a specific geothermal system, it is not clear how universally applicable they are. Apparently similar occurrences of repeated triggering have occurred at other geothermal systems including Yellowstone, the Geysers, and Coso geothermal fields [*Hill et al.*, 1993; *Stark and Davis*, 1996; *Husen et al.*, 2004; *Prejean et al.*, 2004]. At all of these sites, the triggering from Denali began shortly after the initial arrival of the surface waves. Some had later seismic swarms in addition that appeared to begin several hours after the end of the surface waves. Others only had triggered earthquakes while the surface waves were still passing through. None of the other sites have as complete seismic wave data sets as Long Valley.

[47] The most comparable study site is The Geysers geothermal field in northern California. A nonmechanism specific scenario of dependence on stressing wave frequency was proposed by *Gomberg and Davis* [1996] on the basis of their study of triggering at The Geysers. They suggested high-frequency waves were more effective than low-frequency ones, i.e., the opposite dependency as proposed here. Their work was based on trying to explain triggering from input signals like tidal and production-related pumping, which have periods of hours to weeks, with the same threshold relationship as the seismicity induced by seismic waves, which have periods of seconds. The scenario proposed was that there are two competing mechanisms such as a short-timescale pressurization and a long-timescale leakage of pressure that combine to generate the observed high-pass filtering. The above observation and interpretation may be correct at the timescales of hours, weeks and days. It may also help explain why the very small long-period stresses of the seismic waves appear to be effective at triggering earthquakes in Long Valley, even though they are comparable to the background tidal stresses. However, when we confine ourselves to only the seismic bandwidth and reanalyze the Geysers data according to the same methods as used at Long Valley, we find no requirement of a frequency dependence within the seismic frequency band. As there was no broadband seismometer operating in the vicinity of the Geysers when *Gomberg and Davis* [1996] wrote their paper, they compared seismic strains by two different methods: extrapolation from existing stations (at least 144 km away) and generation of synthetics spectra based on source properties. *Gomberg and Davis*'s [1996, Figure 3] extrapolation can be equally well fit by a low-pass as a high-pass filter. The synthetics based on the source spectra are inappropriate for calculating the spectra of the full waveform as important path effects like the amplification of 15–20 s surface waves in the crust are not included.

[48] Another important data set for studying remotely triggered seismicity is the deformation data at Long Valley. After the Landers earthquake, the Long Valley strain meters and tiltmeters show a $\sim$1 month transient [*Hill et al.*, 1993; *Johnston et al.*, 1995]. The Hector Mine and Denali earthquakes generated offsets in strain during the passage of the seismic waves, but did not produce any long-term signals [*Johnston et al.*, 2004]. We have no new direct constraints on the source of the deformation from our strictly seismological study. The proposed unclogging mechanism implies a multitude of pressure sources and sinks in the heterogeneous hydrological system. Such a complex source is consistent with the original interpretation of the deformation data as generated by distributed sources [*Johnston et al.*, 1995].

[49] On the basis of the above observations, we conclude that the model proposed here is consistent with the existing data on geothermal triggering sites in the western United States. However, the paucity of data for sites other than Long Valley leaves the generality of the threshold characteristics open to speculation. The long-period dynamic stresses

that have been observed to trigger seismicity at Long Valley (~5 kPa) are lower than proposed by some earlier studies that did not take into account the frequency effects [*Brodsky et al.*, 2000; *Gomberg et al.*, 2001]. We do not expect that the exact numerical values of the Long Valley thresholds will be universally applicable to sites with varying stress states and seismicity rates, but we speculate that the frequency dependence is a general feature. Time will tell if our prediction is correct.

[50] Long-range triggering has also been proposed in apparently nongeothermal areas such as offshore California, in the central United States and deep subduction zones [*Hough et al.*, 2003; *Tibi et al.*, 2003; *Gomberg et al.*, 2004; *Prejean et al.*, 2004]. The preponderance of long-range triggering observations in geothermal areas suggests that the phenomenon is more likely to occur in these regions, even if it is not exclusively limited to geothermal settings. There may be an observational bias favoring observation of triggering in geothermal areas because dense local networks are often located in these regions. However, careful comparison between the dense Parkfield network and Long Valley after the Landers earthquake illustrates that at least some very active tectonic areas are not prone to long-range triggering [*Spudich et al.*, 1995]. The unclogging mechanism proposed here could potentially work in any setting with water at depth and compliant fault zones, but the mechanism is likely to be more effective in geothermal regions. We speculate that geothermal regions would favor triggering by unclogging for two distinct reasons: (1) the abundance of gases and partially saturated rocks allows large contrasts in storage between hydrological units and (2) the constant precipitation from the evolving geothermal fluids generates fragile blockages in fractures and faults.

5. Summary and Conclusions

[51] Motivated by the proposition that large teleseisms trigger more effectively than the equivalent amplitude shaking from smaller regional events, we used the 12 earthquakes that generated >0.2 cm/s shaking in Long Valley since the installation of the broadband seismometer, to analyze the dependencies of the triggering thresholds at this site. We have narrowed down the possible thresholds for triggering at Long Valley to conclude that: (1) neither amplitude alone nor cumulative shaking determines whether or not triggered earthquakes occur and (2) long-period waves are more effective at triggering than comparable amplitude short-period waves. The second conclusion is based on both the timing of triggering and the observed thresholds. A large part of the frequency dependence is due to attenuation of high-frequency waves at depth. One interpretation of the data is that the triggering occurs by rate-state instabilities in areas where the pore pressure is within 99% of the lithostatic pressure. Triggering could also occur by stress corrosion if the pore pressure is within 99.95% of lithostatic. We consider such extreme pore pressures unlikely, but cannot directly prove or disprove their existence. An alternative interpretation is that the threshold for triggering is constant in time and is most sensitive to the longest-period waves. If so, then the threshold is ~0.05 cm/s vertical shaking at long periods (>30 s) for seismic wave triggering at Long Valley. The frequency effect is consistent with pore pressure being driven in the fault as one stage of the process generating earthquakes. The frequency dependence cannot be explained by any other mechanism as currently formulated, although future work may uncover other possibilities. For now, the low-pass filter can be interpreted as a potential fingerprint of fluid involvement in generating the local earthquakes at Long Valley Caldera.

Appendix A: Correcting the Hector Mine Records

[52] The Tinemaha (TIN) seismic station was within 2° in azimuth of MLAC and 72 km (20%) closer to the source for Hector Mine. The broadband record is clipped at TIN, but the strong motion record at the site remained on scale. We combine attenuation, spreading, radiation pattern and site effects to derive the MLAC ground motion based on the TIN record. The first three corrections are calculated with synthetics calculated by using Thompson-Haskell propagator matrices and a standard southern California model [*Zhu and Rivera*, 2002; *Dreger and Helmberger*, 1993]. The site corrections are done empirically on the basis of the frequency and component-dependent measurements made by *Tinsley et al.* [2004] for earthquakes from 1992 to 2003 combined with our own measurements of amplification of long-period waves averaged over 50 teleseismic events. Frequencies >1 Hz do not contribute significantly to the peak amplitude at TIN for Hector Mine and are therefore not considered. Since MLAC is on soft caldera fill, the site amplification factors generally outweigh the other corrections. The upper bounds on the peak motion at the broadband seismometer MLAC are given by the 1 Hz net amplifications. The lower bounds are the raw TIN records because of the large site corrections.

[53] Later in this paper we apply a low-pass filter to the records. For the low-pass-filtered records, we use the observed range of possible site amplifications to derive a 90% confidence interval on site amplifications for each component. The long-period site amplification has a mean value in the range of 1.2–1.3 for all three components. We combine the site amplification with the geometric spreading factor (0.9) to derive the error bars as shown in Figure 1.

Appendix B: The Parallel Between the Rate-State and Stress Corrosion Governing Equations

[54] The governing equation for evolution of faults with rate-state stress is

$$\frac{\tau(t) - k\delta}{\sigma} = \mu_0' + A \ln \dot{\delta} + B \ln \theta, \tag{B1}$$

where $\tau(t)$ is the forcing stress, σ_n is the background normal stress, k is the stiffness, δ is the slip distance, $\dot{\delta}$ is the slip rate, θ is a state variable and μ_0', A and B are constants. [*Dieterich*, 1994]. The state variable θ evolves as

$$\frac{d\theta}{dt} = 1 - \frac{\theta\dot{\delta}}{D_c}, \tag{B2}$$

where D_c is a constant. It is commonly assumed that $\theta\dot{\delta} \gg D_c$ in the late stages of fault evolution and therefore equations (B1) and (B2) reduce to

$$\frac{\tau(t) - k\delta}{\sigma} = \mu_0' + A \ln \dot{\delta} + B \ln \theta_0 - \frac{B}{D_c}\delta, \tag{B3}$$

where θ_0 is a constant [e.g., *Dieterich*, 1994; *Perfettini et al.*, 2003]. Defining $H \equiv (B/D_c) - (k/\sigma_n)$, the rate-state governing equation simplifies to

$$\frac{\tau(t)}{\sigma} = \mu_0' + A \ln \dot{\delta} + B \ln \theta_0 - H\delta. \tag{B4}$$

[55] The stress corrosion governing equation is

$$\dot{\delta} = \dot{\delta_0}\left(\frac{\delta^{1/2}\tau(t)}{\delta_0^{1/2}\tau_0}\right)^p, \tag{B5}$$

where p is a constant and τ_0 is the initial stress. For the stress corrosion equation, δ is the crack length rather than the slip on a fault. We use the same symbol for both quantities to make the analogous variables easier to identify. Taking the logarithm of both sides and rearranging yields

$$p \ln \frac{\tau(t)}{\tau_0} = \ln \frac{\dot{\delta}}{\dot{\delta_0}} - \frac{p}{2} \ln \frac{\delta}{\delta_0}. \tag{B6}$$

The stress can be separated into initial and changing components, i.e., $\tau(t) \equiv \tau_0 + \Delta\tau(t)$. The exponent p is generally large. A useful limit for large p is

$$\lim_{p\to\infty} (1 + \Delta\tau(t)/\tau_0)^p \to e^{p\Delta\tau(t)/\tau_0}. \tag{B7}$$

A similar manipulation can be done for the crack length where $\delta \equiv \delta_0 + \Delta\delta(t)$. After taking the limits and dividing both sides by p.

$$\frac{\Delta\tau(t)}{\tau_0} = \frac{1}{p} \ln \frac{\dot{\delta}}{\dot{\delta_0}} - \frac{1}{2}\frac{\Delta\delta}{\delta_0} = -\frac{1}{p} \ln \dot{\delta}_0 + \frac{1}{p} \ln \dot{\delta} - \frac{1}{2}\frac{\Delta\delta}{\delta_0}. \tag{B8}$$

[56] Equations (B4) and (B8) are identical mathematically. The constant A is analogous to $1/p$ and H is analogous to $1/2\delta_0$. The initial stress τ_0 for the stress-corrosion system is analogous to σ for the rate-state formulation. $\Delta\tau(t)$ and $\Delta\delta(t)$ act as $\tau(t)$ and $\delta(t)$. The constant term $-\frac{1}{p} \ln \dot{\delta}_0$ in analogous to the combination of constants $\mu'_0 + B \ln \theta_0$. By making these substitutions, we can adopt all of the results for the rate-state system for late stage evolution to the stress corrosion system as long as the $p \to \infty$ assumption is valid.

Appendix C: Fracture Flow Model

[57] We make the simplifying assumption for the flow model that the coupling between the seismic waves and the pore pressure is entirely due to the dilatational strain of the seismic waves. The dilatational strain directly generates a hydraulic head oscillation with the local amplitude dependent on the local stiffness as measured by the specific storage. Since the amplitude of the head oscillations is different in the stiff, intact rock and the damaged fault zone, a flow is generated between the two types of rocks. The flow follows the usual diffusion equation for porous media [e.g., *Philips*, 1991]. We calculate the total head oscillation for the fault, taking into account both the direct oscillation and the flow process.

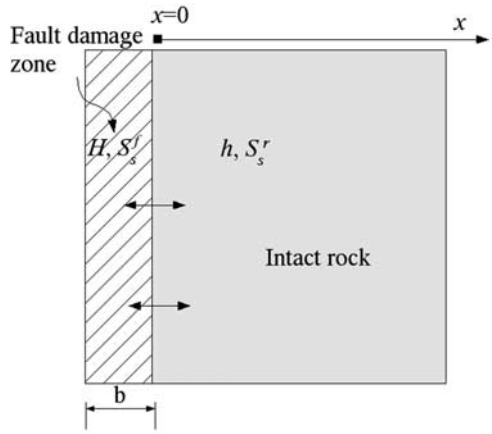

Figure C1. Cartoon of the geometry used in the flow model.

[58] We assume that the fault is an infinite planar feature with half width b (Figure C1). The hydraulic head inside the fault is H and outside is h. The flow is symmetrical about the plane of the fault and therefore we only solve for the flow in the positive x direction. We assume that the head is uniform inside the highly conductive fault. Changes in head inside the fault result from flow of fluid into the fault from the porous media and the forced oscillation of strain. Outside the fault, the flow is governed by Darcy's law and therefore the diffusion equation for head in a porous media with an extra term to account for the forced oscillation. The governing equations are

$$\frac{\partial H}{\partial t} = \frac{K}{bS_s^f}\frac{\partial h}{\partial x} + i\omega\frac{\theta_\infty}{S_s^f}\exp(i\omega t) \tag{C1}$$

$$\frac{\partial h}{\partial t} = \kappa_r\frac{\partial^2 h}{\partial x^2} + i\omega\frac{\theta_\infty}{S_s^r}\exp(i\omega t), \tag{C2}$$

where κ_r is the hydraulic diffusivity of the intact rock, K is the hydraulic conductivity of the intact rock and S_s^f and S_s^r are the specific storages of the fault and intact rock, respectively. Note that in general the hydraulic diffusivity is related to the conductivity and specific storage by $\kappa_r = K/S_s$. The response to an oscillatory strain is assumed to be oscillatory, i.e., the heads are of the form

$$H = H_* \exp i\omega t \tag{C3}$$

$$h = h_* \exp i\omega t, \tag{C4}$$

where H_* and h_* are the amplitudes of the head oscillation in the fault and intact rock, respectively. The boundary conditions are

$$\text{As } x \to \infty, h_* \to \frac{\theta_\infty}{S_s^r} \tag{C5}$$

$$\text{At } x = 0, h_* = H_*. \tag{C6}$$

We substitute equations (C3)–(C4) into equations (C1)–(C2) and solve for h_* to find

$$h_* = \left(H_* - \frac{\theta_\infty}{S_s^r}\right)\exp(-\lambda x) + \frac{\theta_\infty}{S_s^r}, \tag{C7}$$

where

$$\lambda = \sqrt{\frac{i\omega}{\kappa_r}}. \tag{C8}$$

Using the solution for h_* in equation (C7), we solve for H_* and find

$$\frac{H_*}{\theta_\infty} = \frac{1}{S_s^f}\frac{\frac{\sqrt{i\omega\kappa_r}}{b} + i\omega}{\frac{\sqrt{i\omega\kappa_r}}{b}\frac{S_s^r}{S_s^f} + i\omega}, \tag{C9}$$

which is the solution used in equation (10) and Figure 9.

[59] **Acknowledgments.** We are indebted to J. Barker for solutions to the porous media flow problem. Discussions with J. Vidale and M. Hellweg improved our study. Comments from J. Hardebeck and S. Hough improved an early draft of this manuscript. Detailed reviews from J. Gomberg, H. Perfettini, and an anonymous review were a great help in reworking the paper. The California Integrated Seismic Network, Southern Californian Earthquake Data Center and Berkeley Data Center provided the seismic data. The work was funded in part by NSF grant EAR-0238455.

References

Anderson, J., J. Brune, J. Louie, Y. Zeng, M. Savage, G. Yu, Q. Chen, and D. DePolo (1994), Seismicity in the western Great-Basin apparently triggered by the Landers, California, earthquake, 28 June 1992, *Bull. Seismol. Soc. Am.*, *84*, 863–891.

Atkinson, B. K. (1984), Subcritical crack growth in geological materials, *J. Geophys. Res.*, *89*, 4077–4114.

Ben-Menahem, A., and S. J. Singh (1981), *Seismic Waves and Sources*, Dover, Mineola, N. Y.

Blanpied, M., D. Lockner, and J. Byerlee (1995), Frictional slip of granite at hydrothermal conditions, *J. Geophys. Res.*, *100*, 13,045–13,064.

Brodsky, E. E. (2001), Studies in fluid dynamics as applies to seismology and volcanology, Ph.D. thesis, Calif. Inst. of Technol., Pasadena.

Brodsky, E. E., B. Sturtevant, and H. Kanamori (1998), Earthquake, volcanoes and rectified diffusion, *J. Geophys. Res.*, *103*, 23,827–23,838.

Brodsky, E. E., V. Karakostas, and H. Kanamori (2000), A new observation of dynamically triggered regional seismicity: Earthquakes in Greece following the August, 1999 Izmit, Turkey earthquake, *Geophys. Res. Lett.*, *27*, 2741–2744.

Brodsky, E. E., E. Roeloffs, D. Woodcock, I. Gall, and M. Manga (2003), A mechanism for sustained groundwater pressure changes induced by distant earthquakes, *J. Geophys. Res.*, *108*(B8), 2390, doi:10.1029/2002JB002321.

Dieterich, J. (1994), A constitutive law for rate of earthquake production and its application to earthquake clustering, *J. Geophys. Res.*, *99*, 2601–2618.

Dreger, D., and D. Helmberger (1993), Determination of source parameters at regional distances with three-component sparse network data, *J. Geophys. Res.*, *98*, 8107–8125.

Gomberg, J. (2001), The failure of earthquake failure models, *J. Geophys. Res.*, *106*, 16,253–16,263.

Gomberg, J., and S. Davis (1996), Stress/strain changes and triggered seismicity at The Geysers, California, *J. Geophys. Res.*, *101*, 733–749.

Gomberg, J., P. Reasenberg, P. Bodin, and R. Harris (2001), Earthquake triggering by seismic waves following the Landers and Hector Mine earthquakes, *Nature*, *411*, 416–466.

Gomberg, J., P. Bodin, K. Larson, and H. Dragert (2004), Earthquake nucleation by transient deformations caused by the M = 7.9 Denali, Alaska, earthquake, *Nature*, *427*, 621–624.

Hill, D., et al. (1993), Seismicity remotely triggered by the magnitude 7.3 Landers, California, earthquake, *Science*, *260*, 1617–1623.

Hill, D. P., M. J. S. Johnston, and J. O. Langbein (1995), Response of Long Valley Caldera to the M_w = 7.3 Landers, California, earthquake, *J. Geophys. Res.*, *100*, 12,985–13,005.

Hough, S., L. Seeber, and J. G. Armbruster (2003), Intraplate triggered earthquakes: Observations and interpretations, *Bull. Seismol. Soc. Am.*, *93*, 2212–2221.

Hubbert, M. K., and W. W. Rubey (1959), Role of fluid pressure in mechanics of overthrust faulting, *Geol. Soc. Am. Bull.*, *70*, 115–166.

Husen, S., S. Wiemer, and R. Smith (2004), Remotely triggered seismicity in the Yellowstone National Park region by the 2002 M_w = 7.9 Denali Fault earthquake, Alaska, *Bull. Seismol. Soc. Am.*, *94*, S317–S331.

Ichihara, M., E. Brodsky, and H. Kanamori (2003), Reconsideration of the effect of rectified diffusion in volcanic-seismic systems, paper presented at International Union of Geophysics and Geodesy Symposium, Sapporo, Japan.

Jaeger, J., and N. W. Cook (1979), *Fundamentals of Rock Mechanics*, CRC Press, Boca Raton, Fla.

Johnston, M. J. S., D. P. Hill, A. T. Linde, J. Langbein, and R. Bilham (1995), Transient deformation during triggered seismicity from the 28 June 1992 M_w = 7.3 Landers earthquake at Long Valley volcanic caldera, California, *Bull. Seismol. Soc. Am.*, *85*, 787–795.

Johnston, M. J. S., S. Prejean, and D. P. Hill (2004), Triggered deformation and seismic activity under Mammoth Mountain in Long Valley Caldera by the November 3, 2002, M_l 7.9 Denali Fault earthquake, *Bull. Seismol. Soc. Am.*, *94*, S360–S369.

Kanamori, H., and E. E. Brodsky (2004), The physics of earthquakes, *Rep. Progress Phys.*, *67*, 1429–1496.

Kilb, D., J. Gomberg, and P. Bodin (2002), Aftershock triggering by complete Coulomb stress changes, *J. Geophys. Res.*, *107*(B4), 2060, doi:10.1029/2001JB000202.

Linde, A., I. Sacks, M. Johnston, D. Hill, and R. Bilham (1994), Increased pressure from rising bubbles as a mechanism for remotely triggered seismicity, *Nature*, *371*, 408–410.

Love, A. (1927), *Mathematical Theory of Elasticity*, Cambridge Univ., New York.

Perfettini, H., J. Schmittbuhl, and A. Cochard (2003), Shear and normal load perturbations on a two-dimensional continuous fault: 2. Dynamic triggering, *J. Geophys. Res.*, *108*(B9), 2409, doi:10.1029/2002JB001805.

Philips, O. M. (1991), *Flow and Reactions in Permeable Rocks*, Cambridge Univ. Press, New York.

Prejean, S. G., D. P. Hill, E. E. Brodsky, S. Hough, M. Johnston, D. Oppenheimer, M. Pitt, and K. Richards-Dinger (2004), Observations of remotely triggered seismicity on the United States West Coast following the *M*7.9 Denali Fault earthquake, *Bull. Seismol. Soc. Am.*, *94*, S348–S359.

Roy, M., and C. Marone (1996), Earthquake nucleation on model faults with rate- and state-dependent friction: Effects of inertia, *J. Geophys. Res.*, *101*, 13,919–13,932.

Spudich, P., L. K. Steck, M. Hellweg, J. Fletcher, and L. M. Baker (1995), Transient stresses at Parkfield, California, produced by the *M* 7.4 Landers earthquake of June 28, 1992: Observations from the UPSAR dense seismograph array, *J. Geophys. Res.*, *100*, 675–690.

Stark, M. A., and S. D. Davis (1996), Remotely triggered microearthquakes at The Geysers geothermal field, California, *Geophys. Res. Lett.*, *23*, 945–948.

Sturtevant, B., H. Kanamori, and E. E. Brodsky (1996), Seismic triggering by rectified diffusion in geothermal systems, *J. Geophys. Res.*, *101*, 25,269–25,282.

Tibi, R., D. Wiens, and H. Inoue (2003), Remote triggering of deep earthquakes in the 2002 Tonga sequences, *Nature*, *424*, 921–952.

Tinsley, J., S. Hough, A. Yong, H. Kanamori, E. Y. V. Appel, and C. Wills (2004), Geotechnical characterization of TriNet sites, *Seismol. Res. Lett.*, *75*, 505–514.

Winkler, K., and A. Nur (1982), Seismic attenuation: Effects of pore fluids and frictional sliding, *Geophysics*, *47*, 1–15.

Zhu, L., and L. Rivera (2002), A note on the dynamic and static displacements from a point source in multilayered media, *Geophys. J. Int.*, *148*, 619–627.

E. E. Brodsky, Department of Earth and Space Sciences, University of California, 3806 Geology Bldg., Box 951567, Los Angeles, CA 90095, USA. (brodsky@ess.ucla.edu)

S. G. Prejean, Alaska Volcano Observatory, USGS, 4200 University Ave., Anchorage, AK 99508, USA. (sprejean@usgs.gov)